



7

8

9 By projecting surface temperature data (1959-2004) onto the spatial structure obtained

10 objectively from the composite mean difference between solar max and solar min years,

11 we obtain a global warming signal of almost 0.2 °K attributable to the 11-year solar

12 cycle. The statistical significance of such a globally coherent solar response at the

13 surface is established for the first time.

14 **1. Introduction.**

15  
16 Because of the variations of sunspots and faculae on the sun's surface, the total solar  
17 irradiance (TSI), also called the solar constant, varies on a roughly 11-year cycle by about  
18 0.07%, which has been measured by orbiting satellites since 1978 [*Lean*, 1987; , 1991;  
19 *Wilson, et al.*, 1981]. The change in the solar constant amounts to about  $0.90 \text{ Wm}^{-2}$  for  
20 the last three cycles. There have been thousands of reports over two hundred years of  
21 regional climate responses to the 11-year variations of solar radiation, ranging from  
22 cycles of Nile River flows, African droughts, to temperature measurements at various  
23 selected stations, but a coherent global signal at the surface has not yet been established  
24 statistically [*Hoyt and Schatten*, 1997; *Pittock*, 1978]. Since the forcing is global,  
25 theoretically one should expect a global-scale response. When globally and annually  
26 averaged and detrended, but otherwise unprocessed, the surface air temperature since  
27 1959 (when modern rawinsonde network was established) is seen in Figure 1 to have an  
28 interannual variation of about  $0.2 \text{ }^\circ\text{K}$ , somewhat positively correlated with the solar  
29 cycle, although the signal also contains a higher frequency (of 3-5 year period) variation  
30 of comparable magnitude, possibly due to El Niño-Southern Oscillation (ENSO). An  
31 isospectral Monte-Carlo test shows that the correlation coefficient,  $\rho=0.42$ , between the  
32 global temperature and the TSI is statistically significant at 97.4% confidence level. The  
33 “solar cycle signal” obtained by regressing the temperature onto the TSI time series  
34 yields the regression coefficient of  $\kappa=0.12 \pm 0.08 \text{ }^\circ\text{K per Wm}^{-2}$  of solar constant variation,  
35 suggesting a mean global warming of  $\sim 0.1 \text{ }^\circ\text{K}$  from solar min to solar max, which turns  
36 out to be an underestimate, as we will show. This particular result has a large error bar

37 (at  $\pm 2\sigma$  level); so any value between 0.04 to 0.2 °K is allowed. So the problem becomes  
38 how best to filter out the non-decadal variability.

## 39 **2. Composite Mean Difference (CMD) Projection**

40  
41 One powerful approach is to take advantage of the spatial characteristics of the solar-  
42 cycle response. One intuitive way to obtain the spatial pattern is to use the difference of  
43 the solar-max composite and the solar-min composite. Figure 2a shows the meridional  
44 pattern of the composite-mean difference for the zonal-mean, annual-mean air  
45 temperature at the surface using the global dataset of NCEP [Kalnay, *et al.*, 1996],  
46 linearly detrended to remove the secular global-warming signal. Composite differences  
47 have often been used to deduce the pattern of solar-cycle response [Labitzke, *et al.*,  
48 2002]. However, the difficulty lies in verifying the statistical significance of the pattern  
49 generated by this method; since even with an arbitrary partition into any two groups,  
50 there is always a difference pattern. Here we employ an additional step of projecting our  
51 original detrended data onto this spatial pattern, in effect using it as a spatial filter, and  
52 generate a *time* series, shown in Figure 2c. It is seen that this procedure effectively filters  
53 out the higher-frequency ENSO variability. There is now a much higher correlation of  
54 the response with the solar TSI index, with a higher correlation coefficient of  $\rho=0.64$ , and  
55 a 50% higher (mean) regression amplitude of  $\kappa=0.18\pm 0.08$  °K per  $\text{Wm}^{-2}$ .

### 56 **2.1. Statistical significance**

57  
58 We can now test the statistical significance of our “solar-cycle signal” by asking what the  
59 likelihood is that the observed correlation,  $\rho=0.64$ , could be obtained randomly. We  
60 address this question using a bootstrap Monte-Carlo test, which randomly assigns years,

61 with replacement, to the two groups; the result is shown in Figure 2b. It establishes that  
62 the observed correlation of the spatially filtered surface temperature with the 11-year  
63 solar cycle is statistically significant at 99.8% confidence level. This is the first time a  
64 coherent global pattern of response to solar cycles has been shown to be statistically  
65 significant (see the critique of *Coughlin and Tung* [2006] on the spatial pattern of  
66 *Gleisner and Thejll* [2003] obtained through correlation coefficients).

67

68 Early estimates of the solar-cycle response were obtained using *model-generated*  
69 “optimal space-time filter”[*Stevens and North*, 1996] , whose pattern is small over the  
70 poles as compared to the tropics. This may be a reason for the very small global-mean  
71 surface temperature obtained, about 0.06 K, because the pattern obtained *objectively* from  
72 data is very different (see Figure 2a). Other previously used methods, such as multiple  
73 regression methods and composite differences, have not been able to establish a  
74 statistically significant coherent global pattern. In the multiple regression method, the  
75 time series at each spatial location is analyzed independently of the time series from other  
76 locations. Although a spatial pattern of the solar-cycle response can be reconstructed  
77 afterwards by piecing together the regression coefficients for the solar-cycle index from  
78 each location, it turns out that over most of the globe, with the exception of two strips  
79 near the midlatitudes, the signal falls below statistical significance (see *Haigh* [2003] ).  
80 In the work of *Labitzke et al.* [2002], the composite-mean difference obtained by them  
81 was not used in the statistical test of the correlation coefficient. The latter was obtained  
82 separately by correlating the original time series at each location with the solar-cycle  
83 index. These previous methods do not take advantage of the spatial information of the

84 response. We have obtained higher statistical significance by first filtering the time series  
85 through this spatial filter. One variability that our spatial filter may not remove is the  
86 volcanic-aerosol cooling, which probably has a similar global distribution. It however  
87 can be removed in the temporal domain. Volcanic eruptions, particularly El Chichón in  
88 March 1982 and Pinatubo in June 1991, coincidentally occurring during solar maxes,  
89 may contaminate the 11-year signal. The expected cooling in the troposphere for the  
90 transient aerosol events however lasted temporarily, for about two to three years. Since  
91 our method does not require a continuous time series, the volcano aerosol years can be  
92 excluded from the time series. This has been done in Figures 2, where the years 1982 and  
93 1983 (after El Chichón), and 1992 and 1993 (after Pinatubo) are excluded. The  
94 greenhouse warming signal is removed to the extent possible by the linear trend.  
95 However, the linear trend may be sensitive to the end point and unfortunately 2005 is a  
96 very unusual year (one of the warmest on record). To minimize this end-point error, only  
97 1959-2004 were used in the analysis. To include 2005, a nonlinear trend may need to be  
98 used.

### 99 **3. Polar warming**

100  
101 The surface pattern in Figure 2 shows clearly the polar amplification of warming,  
102 predicted by models for the global-warming problem, with largest warming in the Arctic  
103 (3 times that of the global mean), followed by that of the Antarctic (2 times). Since the  
104 tropical atmosphere is more opaque, a warmed surface cannot re-radiate all the energy it  
105 receives back to space. The excess radiative energy must be transported by dynamic heat  
106 fluxes to the high latitudes, resulting in polar warming [*Cai, 2005*]. This occurs rather  
107 quickly, in 5 years or less, and probably involves mostly the atmosphere and the upper

108 oceans, as *White et al.* [1997] showed that the solar-cycle response does not penetrate  
109 deep enough in the ocean to engage the deep water. Low warming occurs over the  
110 latitudes of the Southern ocean and over the Southern tropics. These general features are  
111 similar to those predicted for global warming [*Manabe and Stouffer*, 1980].

#### 112 **4. Amplitude of the global warming**

113  
114 Our work establishes that the surface-temperature response is correlated with the solar-  
115 cycle forcing at over 95% confidence level. For comparison, a similar relationship  
116 between response and forcing has not been statistically established for the greenhouse  
117 global-warming problem. Our result shows a global-mean warming of almost 0.2 °K at  
118 the surface from solar min to solar max. More precisely, we fit  $\delta T = \kappa \delta S$  to all 4.5 solar  
119 cycles, where  $\delta S(t)$  is the TSI variability time series, and find  $\kappa = 0.18 \pm 0.08$  °K/(Wm<sup>-2</sup>)  
120 at the surface. The error bars define a 95% confidence interval and are approximately  
121 equal to  $\pm 2$  standard deviations ( $\sigma$ ). This value of  $\kappa$  is about 50-70% higher than the  
122 regression coefficients of temperature against irradiance variability previously deduced  
123 [*Douglass and Clader*, 2001; *Lean*, 2005; *Scafetta and West*, 2005], of ~0.1 °K global-  
124 mean surface warming attributable to the solar cycles. This result is consistent with the  
125 earlier finding of *Coughlin and Tung* [2004] using a completely different method in the  
126 time domain, who also found the zonal-mean warming to be positively correlated with  
127 the solar-cycle index over most of the troposphere. Our higher response level is also  
128 consistent with some other recent reports [*Haigh*, 2003; *Labitzke, et al.*, 2002; *Van Loon,*  
129 *et al.*, 2004].

130

131 A more novel model, the Linear Discriminant Analysis, can be used to obtain a better  
132 bound with somewhat smaller error bars. The LDA method finds the optimal spatial  
133 structure that best separates the solar-max group from the solar-min group [*Camp and*  
134 *Tung, 2007a; 2007b; Schneider and Held, 2001*]. This result is reported in a forthcoming  
135 paper. The present CMD Projection result has the advantage of being more intuitive and  
136 easier for others to reproduce.

137

## 138 **5. Detailed spatial pattern**

139 Having established the existence of a global-scale solar-cycle response, we next examine  
140 in more detail the surface warming pattern over the globe. We repeat the CMD  
141 Projection analysis on the gridded NCEP surface air-temperature data at a latitude-  
142 longitude resolution of  $5^{\circ} \times 5^{\circ}$ . Consistent with the zonal mean pattern shown in Figure 2,  
143 the largest warming in Figure 3 occurs over the two polar regions. Warming of about 0.7  
144  $^{\circ}\text{K}$  occurs near seasonal sea-ice edges around the Antarctic continent and the Arctic  
145 Ocean, strongly suggestive of a positive ice-albedo feedback as a mechanism for the  
146 polar amplification of the radiative forcing. Although the whole of the western Arctic is  
147 warm, largest warming occurs around the “Northwest Passage” (the Canadian  
148 Archipelago, Beaufort Sea, the coast of northern Alaska and the Chukchi Sea between  
149 Alaska and Siberia). The warm pattern is quite similar to the observed recent trend  
150 [*Moritz, et al., 2002*], and may suggest a common mechanism. In the midlatitudes, there  
151 is more warming over the continents than over the oceans. Most of Europe is warmed by  
152  $0.3^{\circ}\text{K}$ , and eastern Canada by  $0.4^{\circ}\text{K}$ , while western U.S. sees a smaller warming of  $0.2$   
153  $^{\circ}\text{K}$ . Over the tropics, not much warming occurs whether it is over land or over ocean. The

154 warming over the tropics instead occurs higher up, at 200 hPa (not shown, at only 90%  
155 confidence level because of the quality of the upper air data prior to 1979), which is  
156 where the latent heat due to vertical convection is deposited. Cai [2005] discusses how,  
157 the greenhouse warming problem, the vertical transport of surface heating in a moist  
158 atmosphere leads to an increase in poleward heat transport despite the weakening of the  
159 surface-temperature gradient due to polar amplification of warming. In the equatorial  
160 Pacific, there is an anti-El Niño signal of cooling over the eastern Pacific off the coast of  
161 Peru and warming over the west Pacific near Papua New Guinea. This change in  
162 climatology over decadal scales is retained while the difference between El Niño and La  
163 Niña is filtered out by our method. This non-intuitive pattern is explainable using the  
164 ocean “thermostat” mechanism of *Clements et al* [1996], whereby a basin-wide uniform  
165 heating results in a warmer western Pacific, but does not heat the eastern Pacific, which is  
166 controlled by the cold deep water below the shallow thermocline there. The increased  
167 east-west temperature gradient drives a stronger Walker cell during solar max, creating a  
168 La Niña-like ocean pattern. This pattern has been reproduced in the Cane-Zebiac model  
169 and appears to be consistent with paleo records during the Medieval Maximum of solar  
170 activity, and with an opposite pattern during the Maunder Minimum or the colder climate  
171 following a major volcanic eruption [*Mann, et al., 2005*].

172

## 173 **6. Conclusion**

174 We propose that spatial information be used to filter the surface-temperature data to  
175 obtain a cleaner solar-cycle response. At the global scales, an objectively determined  
176 spatial filter can be obtained by the composite difference between the solar-max years

177 and the solar-min years. This filter effectively removes the shorter interannual variations,  
178 such as from ENSO. We obtained a globally averaged warming of 0.2 °K during solar  
179 max as compared to solar min, somewhat larger than previously reported. More  
180 importantly, we have established that the global-temperature response to the solar cycle is  
181 statistically significant at over 95% confidence level. The spatial pattern of the warming  
182 is also of interest, and shows the polar amplification expected also for the greenhouse-  
183 warming problem. The method used here, the CMD Projection, is one of two methods  
184 we have tried that take advantage of the spatial information, the other method being the  
185 LDA method. Although not as optimal as the LDA method, the CMD Projection  
186 possesses most of the advantages of the former while being much simpler to understand  
187 and implement.

188

189 We will argue in a separate paper that the observed warming is caused mostly by the  
190 radiative heating (TSI minus the 15% absorbed by ozone in the stratosphere), when  
191 taking into account the positive climate feedbacks (a factor of 2-3) also expected for the  
192 greenhouse warming problem.

193

## 194 **Acknowledgements**

195 The research is supported by grant ATM-3 32364 from National Science Foundation, Climate Dynamics  
196 Program. We thank Dr. Judith Lean for providing us with her reconstructed TSI and UV time series.

197 **References**

198

199 Cai, M. (2005), Dynamical amplification of polar warming, *Geophys. Research. Lett.*, 32,  
200 L22710,doi:22710.21029/22005GL024481.

201 Camp, C. D., and K. K. Tung (2007a), The influence of the solar cycle and QBO on the  
202 late winter stratospheric polar vortex, *J. Atmos. Sci.*, 64, 1267-1283.

203 Camp, C. D., and K. K. Tung (2007b), Stratospheric polar warming by ENSO in

204 winter: A statistical study, *Geophys. Research. Lett.*, 34, L04809,

205 doi:04810.01029/02006GL028521.

206 Clements, A. C., et al. (1996), An ocean dynamical thermostat, *J. Climate.*, 9, 2190-2196.

207 Coughlin, K., and K. K. Tung (2004), Eleven-year solar cycle signal throughout the  
208 lower atmosphere, *J. of Geophys. Res.-Atmospheres*, 109.

209 Coughlin, K., and K. K. Tung (2006), Misleading Patterns in Correlation Maps, *J.*  
210 *Geophys. Res.*, 111, D24102, doi:24110.21029/22006JD007452.

211 Douglass, D. H., and B. D. Clader (2001), Climate sensitivity of the Earth to solar  
212 irradiance, *Geophys. Research. Lett.*, 16, doi:10.1029/2002GL015345

213

214 Gleisner, H., and P. Thejll (2003), Patterns of tropospheric response to solar variability,  
215 *Geophysical Research Letters*, 30.

216 Haigh, J. D. (2003), The effects of solar variability on the Earth's climate, *Philos. Trans.*  
217 *R. Soc. Lond. Ser. A-Math. Phys. Eng. Sci.*, 361, 95-111.

218 Hoyt, D. V., and K. H. Schatten (1997), *The role of the sun in climate change*, 279 pp.,  
219 Oxford University Press, New York.

220 Kalnay, E., et al. (1996), The NCEP/NCAR 40-year reanalysis project, *Bull. Amer.*  
221 *Meteorol. Soc.*, 77, 437-471.

222 Labitzke, K., et al. (2002), The global signal of the 11-year solar cycle in the  
223 stratosphere: observations and models, *J. Atmos. Solar-Terr. Phys.*, 64, 203-210.

224 Lean, J. (1987), Solar Ultraviolet Irradiance Variations - a Review, *J. Geophys. Res.-*  
225 *Atmos.*, 92, 839-868.

226 Lean, J. (1991), Variations in the Sun's Radiative Output, *Rev. Geophys.*, 29, 505-535.

- 227 Lean, J. (2005), Living with a variable sun, *Phys. Today*, 58, 32-38.
- 228 Lean, J., et al. (1995), Reconstruction of Solar Irradiance since 1610 - Implications for  
229 Climate-Change, *Geophysical Research Letters*, 22, 3195-3198.
- 230 Manabe, S., and R. J. Stouffer (1980), *J. Geophys. Res.*, 85, 5529.
- 231 Mann, M. E., et al. (2005), Volcanic and solar forcing of the tropical Pacific over the past  
232 1000 years, *J. Climate.*, 18, 447-456.
- 233 Moritz, R. E., et al. (2002), Dynamics of recent climate change in the Arctic, *Science*,  
234 297, 1497-1502.
- 235 Pittock, A. B. (1978), A critical look at long-term sun-weather relationships, *Reviews of*  
236 *Geophysics and Space Physics*, 16, 400-420.
- 237 Scafetta, N., and B. J. West (2005), Estimateed solar contribution in the global mean  
238 surface warming using ACRIM TSI satellite composite, *Geophys. Research. Lett.*, 32,  
239 doi:10.1029/2005GL023849.
- 240 Schneider, T., and I. M. Held (2001), Discriminants of twentieth-century changes in earth  
241 surface temperatures, *Journal of Climate*, 14, 249-254.
- 242 Stevens, M. J., and G. R. North (1996), Detection of the climate response to the solar  
243 cycle, *Journal of Atmospheric Sciences*, 53, 2594-2608.
- 244 Van Loon, H., et al. (2004), A decadal solar effect in the tropics in July-August, *J.*  
245 *Atmosp. Solar-Terr. Phys.*, 66, 1767-1778.
- 246 White, W. B., et al. (1997), Response of global upper ocean temperature to changing  
247 solar irradiance, *J. Geophys. Res.-Oceans*, 102, 3255-3266.
- 248 Wilson, R. C., et al. (1981), Observation of solar irradiance variability, *Science*, 211, 700-  
249 702.
- 250
- 251

252 FIGURE LEGENDS

253

254 Figure 1. Annual-mean, global-mean NCEP surface air temperature (1959–2004), in red,  
255 with scale on the left axis. The blue line shows the annual-mean TSI time series [*Lean, et*  
256 *al.*, 1995], updated and provided to us by Dr. J. Lean, with scale on the right axis.  $\kappa$  is the  
257 regression of global-mean temperature response in  $^{\circ}\text{K}$  per each  $\text{Wm}^{-2}$  variation of the  
258 solar constant.  $\rho$  is the correlation coefficient between the global temperature and the  
259 TSI. An isospectral Monte-Carlo test, in which the spectral phase of the temperature (or  
260 the TSI) time series is randomized while preserving the spectral amplitude to generate  
261 3,000 synthetic time series, shows that this positive value of  $\rho$  is not likely to occur by  
262 chance.

263

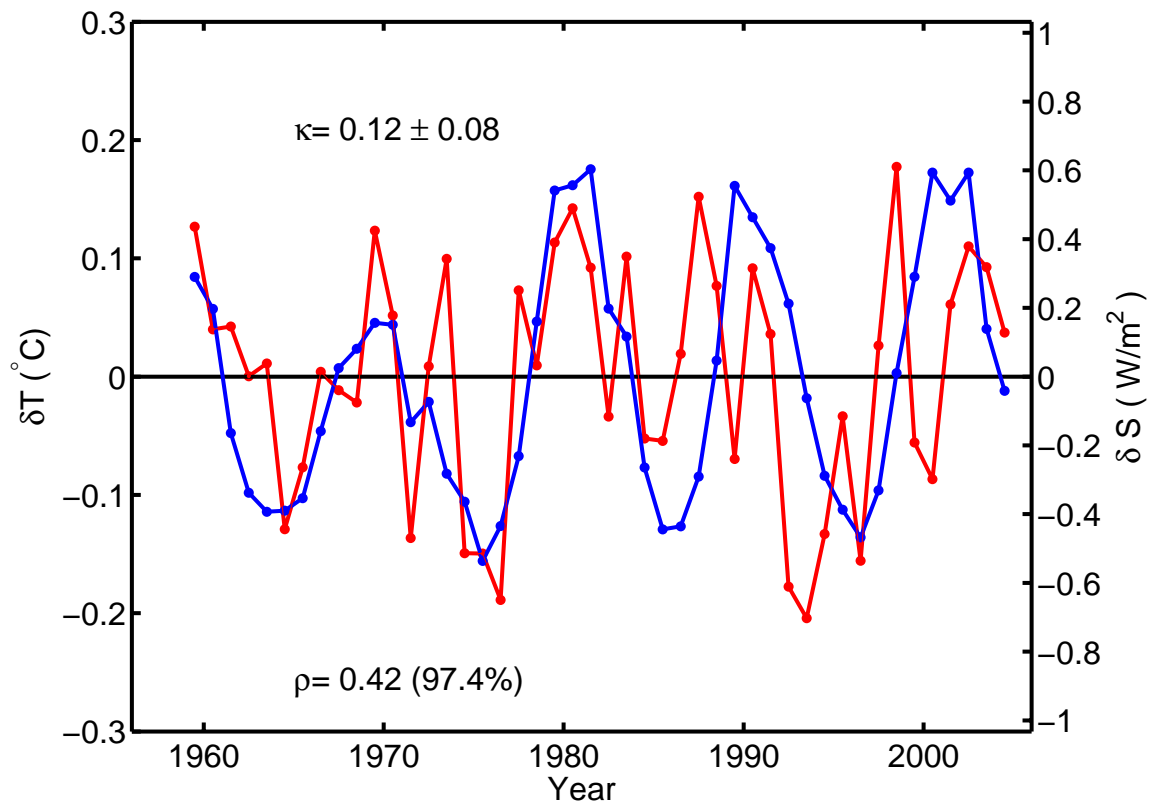
264 Figure 2: Surface temperature from NCEP 1959-2004. (a) The latitudinal pattern of the  
265 zonal-mean annual-mean surface temperature in the years in the solar-max group (when  
266 TSI is  $0.06 \text{ Wm}^{-2}$  above the mean) minus the years in the solar-min group (when TSI is  
267  $0.06$  below the mean), normalized so that its global mean is one. Projecting the original  
268 detrended time series onto the spatial pattern yields the time-dependent index shown in  
269 (c). The red pluses are temperatures in the solar-max group and the blue circles are in the  
270 solar-min group. The black line shows the annual mean TSI time series with scale on the  
271 right axis. The small solid circles indicate the years used in the analysis, while the hollow  
272 small circles indicate the years dropped. These are the years of the volcanoes discussed in  
273 the text. (b) Monte-Carlo test of the correlation coefficient  $\rho$  using 10,000 synthetic time  
274 series of the form of (c) generated using random assignments of the solar-max and solar-  
275 min groups while preserving the same number of years in each group, and projection onto  
276 their composite-mean difference. The observed value of  $\rho=0.64$  is indicated by a vertical  
277 line in (b). It is found to occur by chance only 0.2% of the time.

278

279 Figure 3. The global-surface pattern of temperature obtained by composite-mean  
280 difference (solar-max group minus solar-min group). Shown in color is the temperature  
281 difference in  $^{\circ}\text{K}$  between  $\pm$  one standard deviation from the mean. The actual peak-to-  
282 peak difference between the solar max and solar min is larger, but not as robust as the  
283 standard-deviation difference. A measure of the peak-to-peak difference can be obtained  
284 by multiplying the values shown by a factor of  $\pi/2$ . Monte-Carlo test shows that this  
285 global pattern is statistically significant above the 95% confidence level.

286

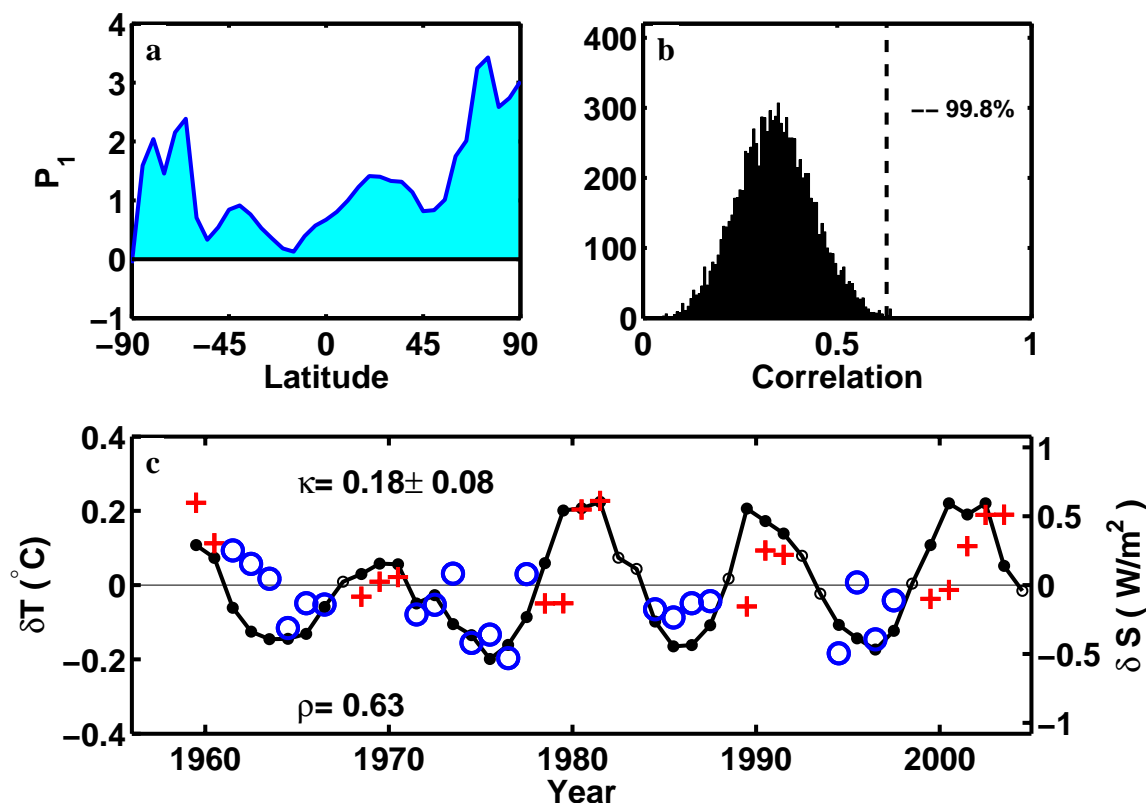
287



288

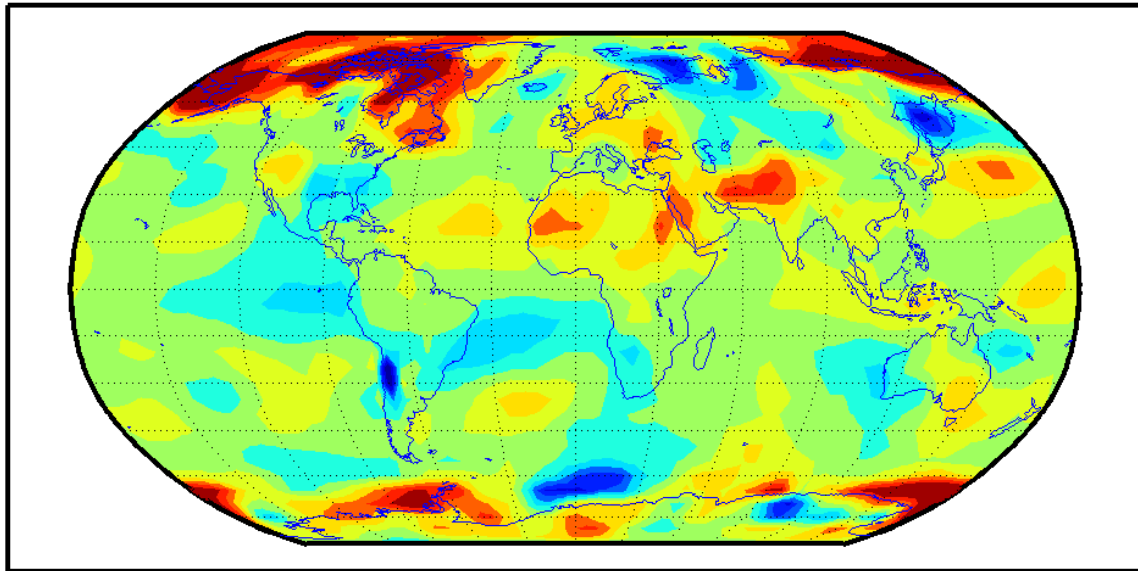
289

290 Figure 1. Annual mean, global mean NCEP surface air temperature (1959–2004), in red,  
 291 with scale on the left axis. The blue line shows the annual mean TSI time series [*Lean, et*  
 292 *al.*, 1995], updated and provided to us by Dr. J. Lean, with scale on the right axis.  $\kappa$  is the  
 293 regression of global mean temperature response in  $^{\circ}\text{K}$  per each  $\text{Wm}^{-2}$  variation of the  
 294 solar constant.  $\rho$  is the correlation coefficient between the global temperature and the  
 295 TSI. An isospectral Monte-Carlo test, in which the spectral phase of the temperature (or  
 296 the TSI) time series is randomized while preserving the spectral amplitude to generate  
 297 3,000 synthetic time series, shows that this positive value of  $\rho$  is not likely to occur by  
 298 chance.

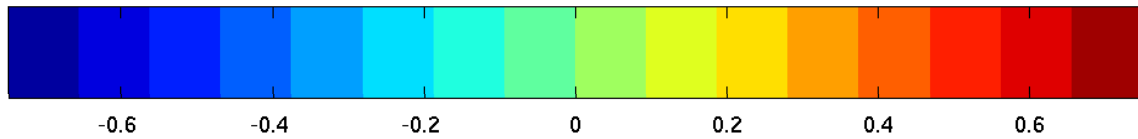


299  
 300  
 301  
 302  
 303  
 304  
 305  
 306  
 307  
 308  
 309  
 310  
 311  
 312  
 313  
 314

Figure 2: Surface temperature from NCEP 1959-2004. (a) The latitudinal pattern of the zonal-mean annual-mean surface temperature in the years in the solar-max group (when TSI is  $0.06 \text{ Wm}^{-2}$  above the mean) minus the years in the solar-min group (when TSI is  $0.06$  below the mean), normalized so that its global mean is one. Projecting the original detrended time series onto the spatial pattern yields the time-dependent index shown in (c). The red pluses are temperatures in the solar-max group and the blue circles are in the solar-min group. The black line shows the annual-mean TSI time series with scale on the right axis. The small solid circles indicate the years used in the analysis, while the hollow small circles indicate the years dropped. These are the years of the volcanoes discussed in the text. (b) Monte-Carlo test of the correlation coefficient  $\rho$  using 10,000 synthetic time series of the form of (c) generated using random assignments of the solar-max and solar-min groups while preserving the same number of years in each group, and projection onto their composite-mean difference. The observed value of  $\rho=0.64$  is indicated by a vertical line in (b). It is found to occur by chance only 0.2% of the time.



°C



315

316

317

318 Figure 3. The global surface pattern of temperature obtained by composite-mean  
 319 difference (solar max group minus solar min group). Shown in color is the temperature  
 320 difference in °K between  $\pm$  one standard deviation from the mean. The actual peak-to-  
 321 peak difference between the solar max and solar min is larger, but not as robust as the  
 322 standard-deviation difference. A measure of the peak-to-  
 323  $\pi/2$ . Monte-Carlo test shows that this global pattern is statistically significant above  
 324 the 95% confidence level.  
 325

326

327